AGU PUBLICATIONS

JGR

Journal of Geophysical Research: Oceans

RESEARCH ARTICLE

10.1002/2016JC012502

Key Points:
- A flood shoal can act as a tidal reflector and limit the influence of an inlet in a multiple-inlet system
- The effects of inertia, friction, and the flood shoal can be separated with a lumped element model
- As an inlet lengthens, narrows, and shoals, the lumped element model shows the initial dominance of the shoal is replaced by friction

Correspondence to:
M. M. Orescanin,
msoresca@nps.edu

Citation:
Orescanin, M. M., S. Elgar, B. Raubenheimer, and L. Gorrell (2017), Effects of a shallow flood shoal and friction on hydrodynamics of a multiple-inlet system, *J. Geophys. Res. Oceans*, *122*, doi:10.1002/2016JC012502.

Received 24 OCT 2016
Accepted 23 JUN 2017
Accepted article online 5 JUL 2017

Effects of a shallow flood shoal and friction on hydrodynamics of a multiple-inlet system

Mara M. Orescanin[1], Steve Elgar[2], Britt Raubenheimer[2], and Levi Gorrell[2]

[1]Oceanography Department, Naval Postgraduate School, Monterey, California, USA, [2]Applied Ocean Physics and Engineering, Woods Hole Oceanographic Institution, Woods Hole, Massachusetts, USA

Abstract Prior studies have shown that frictional changes owing to evolving geometry of an inlet in a multiple inlet-bay system can affect tidally driven circulation. Here, a step between a relatively deep inlet and a shallow bay also is shown to affect tidal sea-level fluctuations in a bay connected to multiple inlets. To examine the relative importance of friction and a step, a lumped element (parameter) model is used that includes tidal reflection from the step. The model is applied to the two-inlet system of Katama Inlet (which connects Katama Bay on Martha's Vineyard, MA to the Atlantic Ocean) and Edgartown Channel (which connects the bay to Vineyard Sound). Consistent with observations and previous numerical simulations, the lumped element model suggests that the presence of a shallow flood shoal limits the influence of an inlet. In addition, the model suggests an increasing importance of friction relative to the importance of the step as an inlet shallows, narrows, and lengthens, as observed at Katama Inlet from 2011 to 2014.

1. Introduction

Primarily owing to friction and geometry, tidal inlets limit the flow of water from the open ocean to back bays, thereby distorting the ocean tidal signal. Many studies of both single- and multiple-inlet systems assume that the back bay is deep relative to the tidal range, and that the length scales of the bay are small relative to the wavelength of the tide [*Keulegan*, 1967; *O'Brien and Clark*, 1974; *Maas and Doelman*, 2002]. Thus, the depth of the back basin has little effect on the hydrodynamics. A topographic high (or tidal divide) in the form of a weir or semi-permeable barrier in the middle of the back bay can restrict the flow between basins, and limit the connectivity between inlets [*Van de Kreeke et al.*, 2008; *De Swart and Volp*, 2012]. However, it is unknown how a substantial flood shoal at the entrance to the bay affects the flow through the inlet and the balance between inlets at a multiple inlet system.

Here, the effects of a shallow flood shoal at the boundary between a tidal inlet and back bay are investigated at Katama Bay, an evolving two-inlet system on Martha's Vineyard, MA (Figure 1). Katama Bay is a small (< 6 km^2), shallow ($\sim$ 1–3 m deep over most of the bay) enclosed body of water that is connected to the Atlantic Ocean via Katama Inlet and to Vineyard Sound via Edgartown Channel (Figure 1b). There is a persistent shallow flood shoal at the transition from Katama Inlet to Katama Bay (Figures 1c and 1d).

The effect of the shallow flood shoal as Katama Inlet migrates, lengthens, narrows, and shoals is investigated with a lumped element model in which the ocean inlet has a geometric step representing the shallow sill. This geometric step creates a mismatch in propagation speed of a shallow water wave, resulting in the partial reflection of the incoming wave. The lumped element model is compared with a linearized 1D momentum balance [*Orescanin et al.*, 2014] and with field observations, and is used to investigate the changing relative roles of friction and of the step between the (relatively) deep inlet and the shallow bay as the inlet morphology evolves.

2. Observations

Sea-surface elevation fluctuations (primarily the M2 tide [*Orescanin et al.*, 2014]) were measured with bottom-mounted pressure gages deployed throughout Katama Bay, Edgartown Channel, Katama Inlet, and the Atlantic Ocean (red squares, Figure 2a) in summer and fall in 2011, 2013, and 2014. Bathymetric (small boat with sonar and GPS) and topographic (hand-pushed dolly with GPS) surveys of the Bay, Edgartown Channel, Katama Inlet, the ebb tidal delta offshore of the inlet mouth, and of the sand spit separating Katama Bay from the Atlantic were performed in 2011, 2013, and 2014.

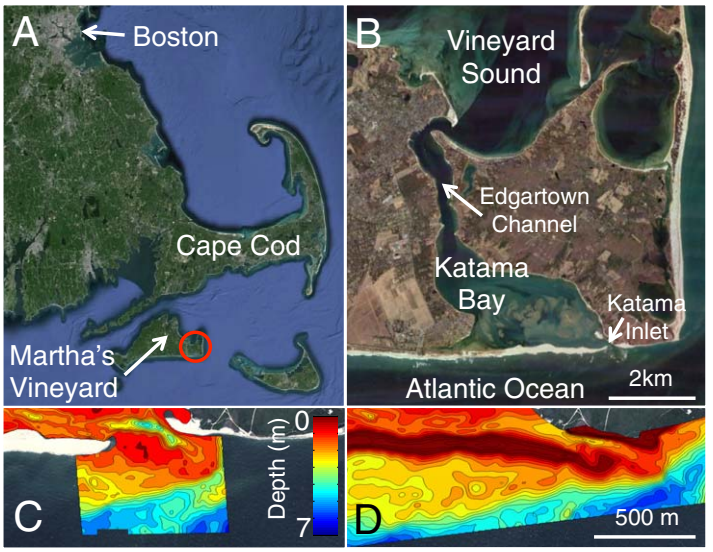

Figure 1. Katama Inlet and surrounding area. (a) Regional map showing location of Katama Bay (red circle). (b) Katama Bay with Edgartown Channel to the north (forced by Vineyard Sound) and Katama Inlet to the south (forced by the Atlantic Ocean). Details of the bathymetry (red is shallow, blue is deep) near Katama Inlet from (c) 2011 post Hurricane Irene and D) 2013 post Hurricane Sandy.

The water depth in Edgartown Channel (Figure 1b) ranges from ~6 m at its mouth in Vineyard Sound (not shown) to ~10 m where it empties into the northern part of Katama Bay (Figures 2a and 2b). The bay depth decreases gradually to the south, where there is an extensive, ~1 m deep flood shoal that connects to Katama Inlet (Figures 2a and 2b). In 2011, Katama Inlet was wide (400 m), deep (5 m), and short (400 m), and was oriented roughly north-south (Figure 1c). Between 2011 and 2013 Katama Inlet migrated several hundred meters to the east (compare Figure 1c with 1d), narrowed (150 m), shoaled (3 m), and lengthened (1000 m), and had rotated so that its orientation was roughly east-west (Figure 1d). The inlet lengthened another 500 m by 2014 (not shown). As Katama Inlet evolved, the flood shoal remained, and there always was a spatially sharp change in water depth between the (relatively) deep inlet and the shallow bay (between locations J and G in Figure 2).

The flood shoal limits the influence of Katama Inlet, and thus of the Atlantic Ocean on sea level in the bay, even when the two inlets have similar cross-sectional areas, as they did in 2011. In 2011 Katama Inlet was 5 m deep, whereas much of the southern half of Katama Bay was less than 1 m deep (Figures 2a and 2b). Relative to the amplitude in Edgartown Channel (location A in Figure 2a, distance=0 in Figure 2c), the amplitude of the M2 component of the observed sea-surface fluctuations decreases slightly across the northern part of the bay (locations A–E, Figure 2c). However, near, and especially within Katama Inlet, tidal

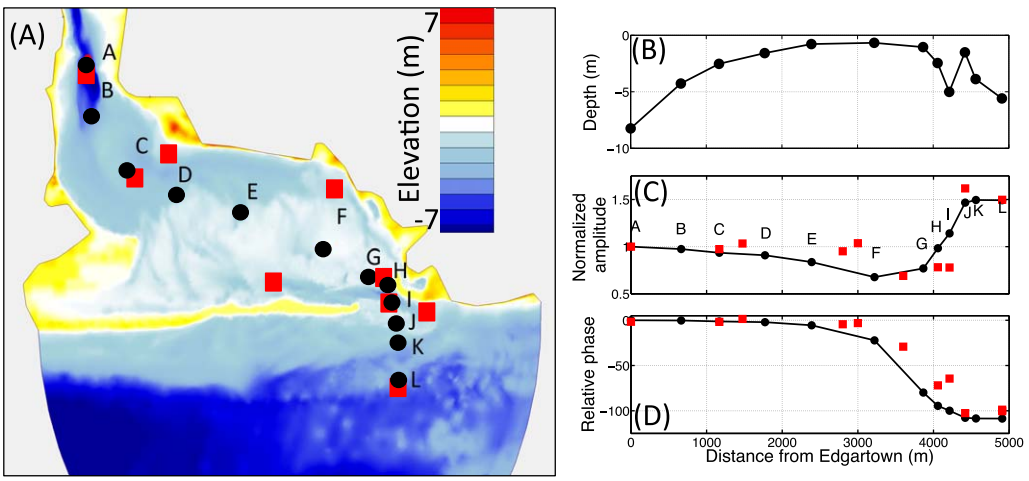

Figure 2. (a) Contours of elevation (relative to mean sea level) (colors, scale on right) in the Katama system in 2011, and (b) water depth, (c) amplitudes (normalized by amplitude at Edgartown at the entrance from Vineyard Sound), and (d) phases of the M2 tidal constituent (relative to that at Edgartown at the entrance from Vineyard Sound) versus distance from Edgartown observed (red squares) and simulated with the 2D depth integrated ADCIRC model (black circles and solid curve). The locations of the observations (red squares) and ADCIRC output (locations A–L) within the inlets and bay are shown in Figure 2a. Katama Inlet is between locations J and G, where the shallow flood shoal begins.

amplitudes change by almost 50% (locations G-J, Figure 2c) before leveling off in the ocean outside of the inlet (locations J–L, Figure 2c), suggesting the majority of the evolution occurs near and within Katama Inlet. Similarly, the phases of the M2 tide relative to that at Edgartown remain nearly constant from north to south across most of the bay, decrease rapidly near the southern edge of the flood shoal and across Katama Inlet (locations F-J, Figure 2d), before leveling off in the ocean outside of the inlet (locations J-L, Figure 2d), suggesting the majority of the evolution occurs near and within Katama Inlet.

Simulations with the two-dimensional depth-averaged numerical model ADCIRC [*Orescanin et al*., 2016] using the measured bathymetry (Figure 2a) and tidal forcing are consistent with the observed spatial structure of the amplitude and phase of the M2 tide across the system (compare black curves and symbols with red symbols Figure 2). However, it is not possible to determine the relative role of the step from ADCIRC.

3. Lumped Element Modeling of Tidal Inlets

To investigate the relative importance of friction, inertia (advection), and the change in depth between Katama Inlet and the flood shoal, a model that includes all three effects is developed. Assuming the tidal wavelength is much larger than the spatial dimensions of the system and that the tidal signal propagates rapidly within the bay such that the bay sea level is uniform, a model using an electrical circuit analogy for which the processes are "lumped" into linear, time-invariant finite elements can be applied to the Katama System, allowing estimation of the causes of the observed changes in circulation as the inlet evolves. The relationship between forcing (tidal water-level fluctuations) and response (currents or discharge) depends on the impedances of each element of the system [*Brown*, 1928; *Keulegan*, 1951, *Van de Kreeke*, 1967, 1988; *Gill*, 1982]. Here, a new term accounting for the impedance caused by the change in depth (the "step") between inlet and bay is developed as a boundary condition between the inlet and bay, and included in the lumped element model.

Lumped element models commonly are used in acoustics and electrical circuit analysis, and also have been used in hydrodynamic systems [*Miles and Munk*, 1961; *Miles*, 1971; *Miles*, 1974; *Miles and Lee*, 1975; *Herman*, 2007]. Using either the concept of a repletion coefficient [*Keulegan*, 1951, 1967; *O'Brien and Clark*, 1974], or acoustical (a Helmholtz resonator [*Miles and Lee*, 1975; *Maas*, 1997; *Stanev et al*., 2003; *Herman*, 2007] or electrical [*Miles*, 1971; *Miles*, 1974; *Miles and Lee*, 1975]) analogies for the impedance, these models can provide computationally efficient, accurate estimates of phase-resolved sea levels and depth-averaged velocities within geometrically complicated inlet-bay systems. Lumped element models have been used to investigate differing ocean tidal amplitudes and phases at multiple inlets [*Herman*, 2007], bay and inlet geometries in multiple-inlet systems [*Ridderinkhof*, 1988], hypsometry (time-varying cross-sectional area and wetted surfaces) [*Stanev et al*., 2003; *de Boer and Maas*, 2011], and topographic highs in the middle of the basins [*Maas*, 1997; *Herman*, 2007; *Van de Kreeke et al*., 2008; *Waterhouse et al*., 2011; *De Swart and Volp*, 2012].

3.1. Lumped Element Model for a Single-Inlet System

A lumped element model for a tidal inlet can be derived by combining conservation of mass and momentum into a single linear and time invariant (coefficients in the ODE are independent of time and space) equation for the bay water-level response to ocean water-level forcing. There are two variables associated with each element, one "across" the element and one "through" the element. In an analogous electrical circuit, the across variable is the voltage and the through variable is the current. For a hydrodynamic system, the variable passing across the element is pressure (sea level) and the variable passing through the element is discharge (volume velocity). The complex impedance relates the driving pressure to the discharge, and ultimately to the sea level inside the bay.

Here it is assumed that Coriolis forces, freshwater discharge, and stratification are negligible, and that frictional effects (generation of tidal harmonics) in the bay, where currents are weak, are small relative to those in the inlets, where currents are strong. The inlets and bay are small relative to the wavelength of the forcing body of water (the M2 tide), and thus it is assumed that the bay water level is spatially uniform, consistent with the observation that there is little evolution of tidal amplitude or phase across the bay (red symbols between A and F in Figures 2c and 2d). The surface areas of the bay and relatively steep-sided inlets do not change significantly ($<$20%) over a tidal cycle, so the effects of hypsometry [*Speer and Aubrey*, 1985; *Stanev*, 2003; *Terra et al*., 2005; *Herman*, 2007; *De Swart and Volp*, 2012] are neglected, and A_B and all inlet dimensions are assumed to be constant in each year. Under these assumptions, the continuity equation is

$$\frac{d\eta_B}{dt} = \frac{U_I(t)}{A_B} \tag{1}$$

where $\eta_B(t)$ is the sea level in the bay, t is time, $U_I(t)=A_I u_I$ is the time-dependent discharge through the inlet (depth- and width-integrated), A_I is the time-averaged cross-sectional area of the inlet of width b_I and depth h_I, u_I is the depth- and width-averaged velocity, and A_B is the surface area of the bay. Similarly, assuming the inlet and bay depths are constant, $h_I=h_B$ (a boundary condition) and a rectangular inlet, the depth-averaged momentum equation integrated along the length of the inlet is

$$\frac{dU_I}{dt} = gA_I\frac{(\eta_o-\eta_B)}{L_I} - C_d\frac{\overline{|u_I|}}{h_I}U_I \tag{2}$$

where g is gravitational acceleration, $\eta_o(t)$ is the sea level in the ocean (forcing), L_I is the effective length of the inlet (to include the effect of entrance and exit losses), C_d is the friction coefficient, and $\overline{|u_I|}$ is the temporal average of the absolute value of the time varying mean velocity (depth and width averaged). Eliminating discharge (U_I) between equations (1) and (2), and assuming linearized friction [*Stanev*, 2003; *Terra et al*., 2005; *Malhadas et al*., 2009] yields

$$\frac{gA_I}{A_B L_I}\eta_o = \frac{d^2\eta_B}{dt^2} + \frac{C_d\overline{|u_I|}}{h_I}\frac{d\eta_B}{dt} + \frac{gA_I}{A_B L_I}\eta_B \tag{3}$$

The ordinary differential equation (3) has the same form as a damped driven harmonic oscillator and as a Helmholtz resonator (see *Kinsler et al*. [1976] for an acoustic example).

The system is driven by a forcing tide $\tilde{\eta}_0=\hat{\eta}_0 e^{j(\omega t+\varphi_0)}$, where $\tilde{\eta}_0$ is the complex ocean forcing (the complex form is retained for simplicity of solving the ODE) with complex amplitude, $\hat{\eta}_0$, and φ_0 is the phase difference between the ocean and bay. Note that the complex form for sea level solves equation (3), and therefore satisfies equations (1) and (2), which are derived for real sea levels, η_o and η_B, and real discharge, U_I. For long waves (relative to the dimensions of the inlet and bay) the spatial component of the forcing term is neglected, and thus assuming a complex solution of the form $\tilde{\eta}_B=\hat{\eta}_B e^{j\omega t}$, equation (3) becomes

$$\frac{gA_I}{A_B L_I}\hat{\eta}_0 e^{j(\omega t+\varphi_0)} = -\omega^2\hat{\eta}_B e^{j\omega t} + j\omega\frac{C_d\overline{|u_I|}}{h_I}\hat{\eta}_B e^{j\omega t} + \frac{gA_I}{A_B L_I}\hat{\eta}_B e^{j\omega t} \tag{4}$$

where ω is radian frequency, and $j=\sqrt{-1}$. If $\tilde{\eta}_B \propto e^{j\omega t}$ is a solution, then so is (by conservation of mass) $A_B\frac{\partial\tilde{\eta}_B}{\partial t}=\tilde{U}_I \propto j\omega e^{j\omega t}$, where $\tilde{U}_I$ is the complex discharge through the inlet. The complex impedance is a transfer function that relates the discharge response to the pressure forcing (tides), and is defined as $Z=\tilde{P}/\tilde{U}_I$, where $\tilde{P}=\rho g\tilde{\eta}_0$ is the complex pressure in the ocean, with ρ the density of water, and $\tilde{\eta}_0$ is the complex surface elevation in the ocean [*Gill*, 1982] ($\tilde{U}_I=A_I\tilde{u}_I=A_B\frac{d\tilde{\eta}_B}{dt}=A_B j\omega\hat{\eta}_B e^{j\omega t}$ from conservation of mass). The complex impedance can be obtained for the single inlet system by multiplying equation (4) by $\rho L_I/A_I$ and dividing by $\tilde{U}_I=j\omega\hat{\eta}_B e^{j\omega t}$, yielding

$$Z=\frac{\tilde{P}}{\tilde{U}_I}=\frac{\rho g\hat{\eta}_0 e^{j\varphi_0}}{j\omega A_B\hat{\eta}_B}=j\omega\rho\frac{L_I}{A_I}+\frac{\rho C_d\overline{|u_I|}}{h_I}\frac{L_I}{A_I}+\frac{\rho g}{j\omega A_B}=Z_M+Z_R+Z_C \tag{5}$$

Continuing the analogy to an electrical circuit or an acoustical Helmholtz resonator where $Z=j\omega M+R+{}^{1}/_{(j\omega C)}$, the hydrodynamic system $M=\frac{\rho L_I}{A_I}$ is related to the mass of oscillating water in the inlet (similar to inertia in a momentum balance), $R=\frac{C_d\overline{|u_I|}}{h_I}\frac{\rho L_I}{A_I}$ is friction, and $C=\frac{A_B}{g\rho}$ is the resistance caused by increasing or decreasing the water level in the bay (for the acoustical analogy, see *Kinsler et al*. [1976]).

Solving for the bay sea level in the inlet system (Figure 3a) is equivalent to solving for the voltage, V_B, in an electrical analogy (Figure 3b) [*Miles*, 1971, 1974; *Miles and Lee*, 1975]. The solution for the complex bay sea level is

$$\tilde{\eta}_B(t)=\frac{\tilde{U}_I}{\rho g}Z_C=\frac{Z_C}{Z_M+Z_R+Z_C}\tilde{\eta}_0(t) \tag{6}$$

where $\tilde{U}_I/\rho g=\tilde{\eta}_0(t)/(Z_M+Z_R+Z_C)$ is the balance between inlet discharge, $\tilde{U}_I$, and forcing water level, $\tilde{\eta}_0$, using the impedance $\left(Z=\tilde{P}/\tilde{U}_I\right)$. The observable sea level in the bay that satisfies equations (1) and (2) is

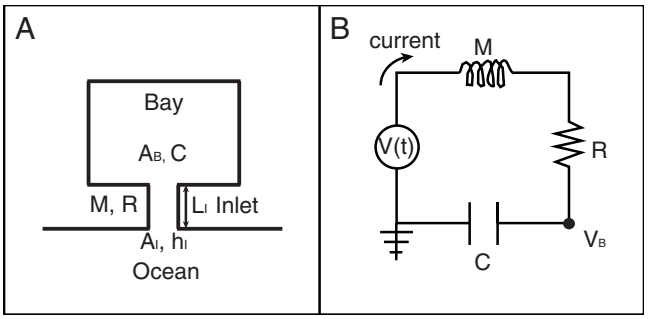

Figure 3. Schematics of (a) a bay with surface area A_B and compliance C connected to the ocean through a single inlet with dimensions A_I and L_I forced by sea level in the ocean, and (b) an electrical circuit representation for the single-inlet system. The elements M, R, and C in Figure 3a correspond to the electrical components in Figure 3b. The solution for the bay sea level, η_B in Figure 3a is equivalent to the solution for the voltage V_B in Figure 3b (real part of equation (6)].

$\eta_B(t)=Re(\tilde{\eta}_B(t))$, in response to the ocean tide $\eta_0(t)=Re\left(\tilde{\eta}_0(t)=\hat{\eta}_0 e^{j(\omega t+\varphi_0)}\right)$. Similarly, the inlet discharge is $U_I(t)=Re\left(\tilde{U}_I(t)\right)$

3.2. Lumped Element Model for a Multiple-Inlet System With a Reflective Step

Given the elements defined for inlet-specific inertances and resistances and for bay-specific compliances, an equivalent electrical circuit can be implemented that accounts for combinations of inlets and bays in series and parallel [*Miles*, 1971; *Miles and Lee*, 1975; *Stanev et al.*, 2003; *Herman*, 2007, *De Swart and Volp*, 2012], such as the Katama system (Figure 4). Here, each inlet satisfies a momentum balance (equation (2)) across it with a boundary condition at the bay, and a new form of equation (1) that includes the discharges from both inlets couples the two momentum balances $\left(A_B\frac{\partial\eta}{\partial t}=U_{I,1}+U_{I,2}\right)$. The inlets are far from each other, and thus their effects are added linearly. The inlets, each with its own forcing and impedance, are coupled via the compliance of the single bay (Figure 4b).

The momentum equation (equation (2)) assumes the boundary condition that the bay and inlet have the same depth. When this boundary condition is modified such that $h_B \neq h_I$, the abrupt change in depth (a step) creates a difference in the phase speed ($c=\sqrt{gh}$) of a shallow ($kh < 1$, where k is the wavenumber) water wave, resulting in partial reflection of the incoming energy, and thus impeding the flow. The step-induced impedance, Z_S (Figure 4b) of each inlet is given by (Appendix A)

$$Z_S=\frac{\rho c_B}{h_B b_I}-\frac{\rho c_B}{h_I b_I}\sqrt{\frac{h_B}{h_I}}=\frac{\rho c_B}{b_I h_B}\left(\frac{h_I^{3/2}-h_B^{3/2}}{h_I^{3/2}}\right) \tag{7}$$

where $c_B=\sqrt{gh_B}$ is the celerity of the tide in the bay. If $h_I=h_B$ then $Z_S \to 0$, because there is no impedance mismatch without a change in depth (no step) at the intersection of inlet and bay. If $h_B \to 0$, then $Z_S \to \infty$, because water cannot enter the bay through the inlet. As $h_B \to \infty$, the solution no longer is valid. The sign of Z_s implies that if $h_I > h_B$ (as in the Katama system), the amplitude response of the bay water level is reduced, and if $h_I < h_B$ the amplitude response of the bay is amplified.

Similar to the one-inlet system, the other components of the impedance caused by the inlet (i.e., not including the bay compliance, C) are owing to friction (R) and to inertia (M), and the total complex impedance caused by an inlet, Z_I, can be written as

$$Z_I=j\omega M+R+Z_S=Z_M+Z_R+Z_S \tag{8}$$

The addition of Z_S to the inlet impedance adds an additional condition to be satisfied for that inlet (Appendix A) to ensure conservation of energy flux across the step. Given that the total inlet impedance, Z_I, is complex, it is necessary to solve for the complex water level, $\tilde{\eta}_B$. The complex water level in the bay, $\tilde{\eta}_B$, can be determined from conservation of mass (discharge, $\tilde{U}_{tot}=\tilde{P}_{bay}/Z_C=\tilde{U}_{I,1}+\tilde{U}_{I,2}$) in the two-inlet system, given by

$$\frac{\tilde{\eta}_B-\tilde{\eta}_1}{Z_{I1}}+\frac{\tilde{\eta}_B-\tilde{\eta}_2}{Z_{I2}}+\frac{\tilde{\eta}_B}{Z_C}=0 \tag{9}$$

where $\tilde{U}_*=\rho g\Delta\tilde{\eta}/Z_*$ and the * refers to the quantity at each inlet. In equation (9), the first two terms account for discharge through each inlet (driven by different tides), and the third term accounts for the change in water level in the bay. Solving equation (9) for $\tilde{\eta}_B$ yields

$$\tilde{\eta}_B=\frac{Z_C Z_{I2}\tilde{\eta}_1+Z_C Z_{I1}\tilde{\eta}_2}{Z_C Z_{I2}+Z_C Z_{I1}+Z_{I1}Z_{I2}} \tag{10}$$

The impedances are determined by parameters of the system (the terms in equations (5) and (8)) specific to a given inlet system, and $\tilde{\eta}_1$ and $\tilde{\eta}_2$ are the complex forcing sea levels at each inlet with their respective amplitudes, a_*, and phases, φ_*, allowing the complex bay sea level, $\tilde{\eta}_B$, to be determined with equation (10).

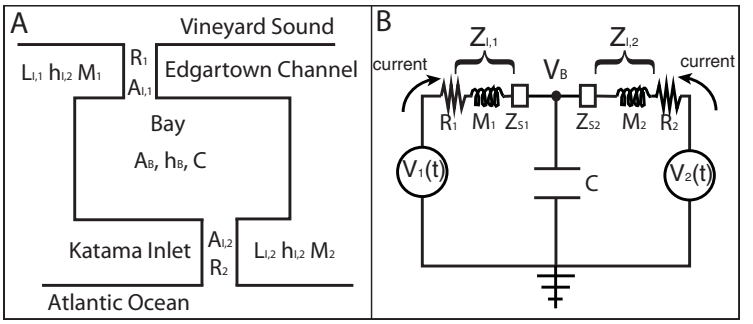

Figure 4. Schematics of (a) a bay with two inlets and (b) an analogous electrical circuit. Elements for a lumped element model are C, M_1, M_2, Z_{S1}, Z_{S2}, R_1, and R_2, where the subscripts 1 and 2 refer to the specific inlet. The hydrodynamic system in Figure 4a is forced by sea levels in Vineyard Sound and the Atlantic Ocean, which are independent of each other. Similarly, the electrical system in Figure 4b is forced by voltages that are independent of each other. The voltage V_B in (B) corresponds to the sea level η_B in the bay in Figure 4a. The element C, related to the effects of filling and emptying the bay (e.g., an acoustical compliance or an electrical capacitance), couples the forcing from both inlets.

The sea level response in the real domain is the real component of equation (10),. The characteristic flows in the inlets, u_{I*} are from observations or estimates. For the case of a real driving pressure (e.g., ocean tides), the response of the bay is the real part of equation (10).

4. Application to the Katama Bay System

To determine the relative roles of friction and of the step as the inlet morphology evolves, the lumped element model (equation (10)) is forced at the inlets with the M2 tidal amplitudes and phases observed in Vineyard Sound (northern inlet) and in the Atlantic Ocean (southern inlet), and solved for the sea level in the bay (Figure 4a). A reflective step is considered only at Katama Inlet where the change in depth is over a short distance.

As the relative size of the step between inlet and bay $((h_I - h_B)/h_I)$ increases, the influence of the inlet on the bay decreases, and the amplitudes and phases of the M2 tide in the bay approach those of Edgartown Channel (inlet 1) (Figure 5). The reduced connectivity between the two inlets owing to the step is similar to the reduced connectivity owing to a topographic high [*Maas*, 1997; *Herman*, 2007; *Van de Kreeke et al.*, 2008; *Waterhouse et al.*, 2011; *De Swart and Volp*, 2012], although the mechanisms are different (reflection at a step versus reduced transmission owing to a weir). For a system with dimensions similar to Katama, the influence (impedance) of the step increases as the depth of the bay decreases [compare red with green with blue curves in Figure 5 for any particular $((h_I - h_B)/h_I)$].

The influence of the step (Figure 6, compare green with red symbols) decreased as the ratio of inlet length to cross-sectional area at Katama Inlet increased between 2008 and 2013 (Table 1). In 2008 and 2011, the amplitude and phase of the M2 tide in the bay simulated by the lumped element model without a step (red

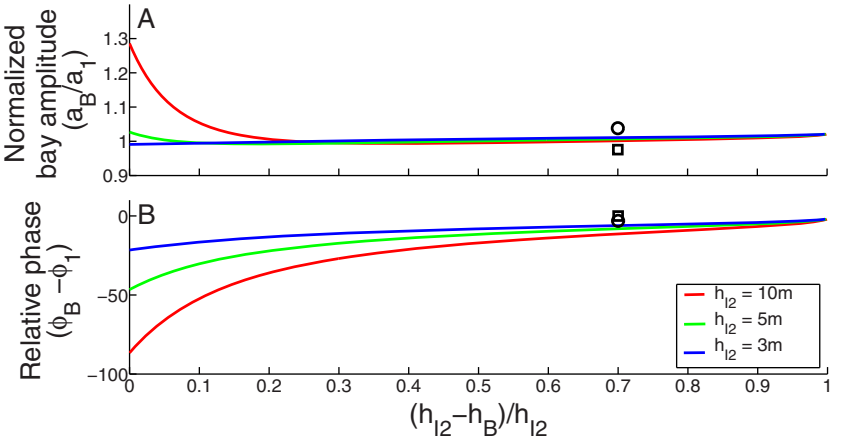

Figure 5. Lumped element model simulations of the bay ($h_B = 1$ m) (a) M2 amplitude (normalized by the amplitude of the M2 forcing at Edgartown, a_1, the second inlet) and (b) phase (relative to the M2 phase in Edgartown) versus relative step height for three inlet depths (listed in the legend) for the 2011 dimensions. As the relative step size, $[(h_I - h_B)/h_I]$, approaches 1, the inlet no longer affects the sea level in the bay. The symbols are values observed at the northern (location C in Figure 2, circles) and eastern (location F, squares) sides of Katama Bay in 2011 $(h_I - h_B)/h_I = 0.7$]. Magnitude and phase for the lumped element model are taken from the complex form of equation (10).

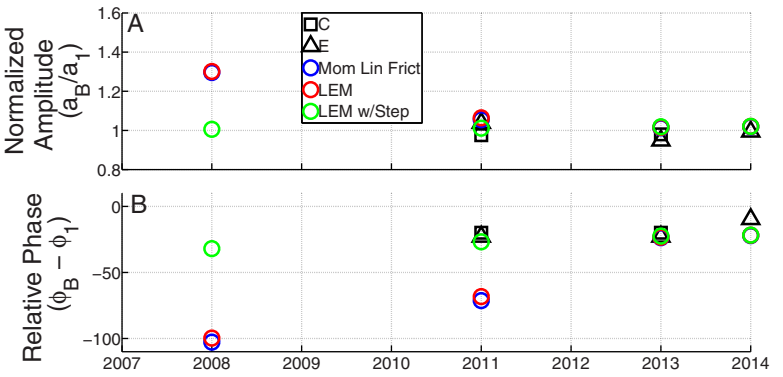

Figure 6. (a) Amplitude and (b) phase of the M2 tidal constituent in the bay relative to those at Edgartown (inlet 1) versus time observed in the north (black squares, near location "C" in Figure 2a) and center (black triangles, near location "E" in Figure 2A) of the bay, modeled by a 1-D momentum balance [*Orescanin et al.*, 2014] with linearized friction (blue), and modeled with the lumped element model with (green) and without (red) a step. Magnitude and phase for the lumped element model are taken from the complex form of equation (10).

circles in Figure 6, identical to the linearized version of the 1-D momentum balance model without a step (blue circles) [*Orescanin et al.*, 2014]) is different than the M2 amplitude and phase simulated by the model with a step (green circles in Figure 6). The model with the step (green) more accurately simulates the observations (black symbols in Figure 6) in 2011, but all models are similar to the data in 2013, implying the relative importance of the step is reduced, likely owing to the increased importance of friction as the inlet lengthens, narrows, and shoals [*Orescanin et al.*, 2016].

The lumped element model allows the relative importance of the components of the impedance (equation (8)) to be assessed as a function of time (Figure 7). Between 2008 and 2011, the magnitude of the Katama Inlet impedance is dominated by the step (green curve in Figure 7), but as the inlet evolved between 2011 and 2013, friction (blue curve in Figure 7) became as important as the step. The additional lengthening and shoaling of the inlet in 2014 resulted in a much stronger influence of friction (compare blue curve with green curve in Figure 7 for 2014).

5. Conclusions

Results from a lumped element model based on geometrical parameters of a multiple-inlet system suggest that the impedance to flow caused by an inlet is a combination of effects from inertia (accelerating a mass of water), friction, and a sill or step between the (relatively) deep inlet and the shallow bay. The presence of a shallow flood shoal at a wide, short inlet decreases the importance of the inlet to the bay by increasing the impedance to the inlet flow. The sea-level response of the bay can be approximated with this analytical method given dimensions of the bay and inlets, water density, drag coefficients, and characteristic inlet velocities. By incorporating a shallow flood shoal, represented as a step, the model simulations are consistent with observations at the two-inlet system of Katama Bay, Martha's Vineyard, MA. The result of the increased impedance from the step at Katama Inlet in 2011 is observed in the nearly 90 degree phase difference of tidal elevation between the model with and without the step, causing the Bay tides to be nearly identical to Vineyard Sound. As the step between Katama Inlet and Katama Bay

Table 1. Dimensions of Katama Inlet (Inlet 2)[a]

	2008	2011	2013	2014
L_{I2} (m)	200	200	800	1500
b_{I2} (m)	1000	400	150	150
h_{I2} (m)	6	5	3	2

[a]Dimensions from 2008 are estimated from satellite imagery. Dimensions from 2011 to 2014 are from satellite imagery and bathymetric surveys. Edgartown Inlet (inlet 1) dimensions are held constant at L_{I1}=3500, b_{I1}=300, and h_{I1}=8 m. Other input parameters [*Orescanin et al.*, 2014, 2016] are: C_{d1}=0.007, C_{d2}= 0.043, ρ=1032 kg/m^3, A_B = 7.5 x 10^6 m^2, h_B=1.0 m, a_1=0.23 m, a_2=0.40 m, φ_1=346.22°, φ_2=231.86°, $\overline{|u_{I1}|}$=0.19 m/s, and $\overline{|u_{I2}|}$ =0.76 m/s. Amplitudes and phases of the M2 driving tides are estimated from measurements in Vineyard Sound and the Atlantic Ocean using t_tide [*Pawlowicz et al.*, 2002], and the currents u_{I1} and u_{I2} are estimated from observations in the inlets.

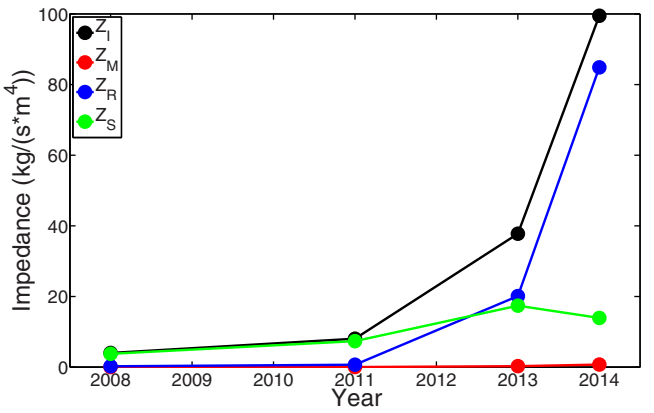

Figure 7. Magnitude of the complex impedance components (equation (8)) of Katama Inlet versus time. The magnitude of the total inlet impedance (Z_I, black) consists of impedances owing to the physical dimensions of the inlet (inertia) (Z_M, red), friction (Z_R, blue), and the step (Z_S, green).

became larger or as the ratio of inlet length to cross-sectional area increased, the flow through the inlet was increasingly impeded, reducing the influence of the Atlantic Ocean, and increasing the influence of Vineyard Sound on water levels in Katama Bay. By separating frictional effects from the impedance caused by the step, the lumped element model suggests an increasing importance of friction relative to the importance of the step as Katama Inlet lengthened, narrowed, and shoaled, consistent with observations and previous numerical model results.

Appendix A: Inlet Impedance From Back Bay Bathymetry

If the bay is shallower than the inlet ($h_I > h_B$), the ocean tidal wave partially is reflected by the rapid change in depth (a "step"), impeding the flow into the bay. At the interface between the inlet and bay, the dynamic boundary condition is that energy flux must be conserved and the kinematic boundary condition is that the sea levels must match. The analysis for both the single and multiple inlet systems presented here assumes the boundary of the bay is reflective, and thus the wave is standing, creating a spatially uniform water level in the bay [*Miles and Munk*, 1961; *Lee and Xing*, 2010]. Higher-order reflections from the bay sides are not considered.

In shallow water with no geometric constraints, neglecting frictional effects, and with a wave traveling in one direction, the pressure associated with the wave, $P=\rho g\eta$, where P is the (complex) pressure, ρ is the density of the water, g is gravity, η is the (complex) wave-induced sea-level fluctuation. This (complex) pressure is compared with the particle velocity of the wave [*Dean and Dalrymple*, 1991], $u=c\frac{\eta}{h}=\sqrt{gh}\frac{\eta}{h}$, where c is the phase velocity of the wave and h is the mean water depth, to determine the specific hydrodynamic impedance z_H [*Kinsler*, 1976; *Gill* 1982; *Dalrymple and Martin*, 1992], given by

$$z_H=\frac{P}{u}=\frac{\rho gh}{c}=\rho c \tag{A1}$$

The analysis of equation (A1) is valid for both complex and real pressures and particle velocities, and the word complex is in () to state this. When geometry is important, such as at an inlet, the hydrodynamic impedance, $Z_H={}^{z_H}/_{A_I}$, is the transfer function between pressure and discharge, where A_I is the cross-sectional area of the inlet, and $U_I=uA_I$ is the (complex) discharge through the inlet.

The change in depth between the inlet and bay results in partial transmission and partial reflection of the incoming tide (Figure A1). The boundary conditions at the transition ($x=0$) are that the sea levels, η, and the energy fluxes, $E_f=Ec_g=\frac{1}{2}\rho g a_*^2 c_g$, are the same on both sides. Here, E is the energy of the wave, c_g is the group velocity of the wave (equal to the phase speed, $c=\sqrt{gh}$, for shallow water waves), and a_* is the amplitude of the sea level, η.

Assuming a sinusoidal sea level (can be generalized for multiple frequencies or in complex form) of the form $\eta_*=a_* sin(\omega t+k_* x)$, where the * subscript can be for the incident, reflected, and transmitted waves, ω is the angular frequency of the incident wave, t is time, and k_* is the wavenumber. The boundary conditions at the transition, $x=0$, are (sea level)

$$\eta_{x=0-}=\eta_{x=0+} \tag{A2}$$

$$a_i+a_R=a_T \tag{A3}$$

and (energy flux),

$$\sqrt{gh_I}b_I a_i^2-\sqrt{gh_I}b_I a_R^2=\sqrt{gh_B}b_I a_T^2 \tag{A4}$$

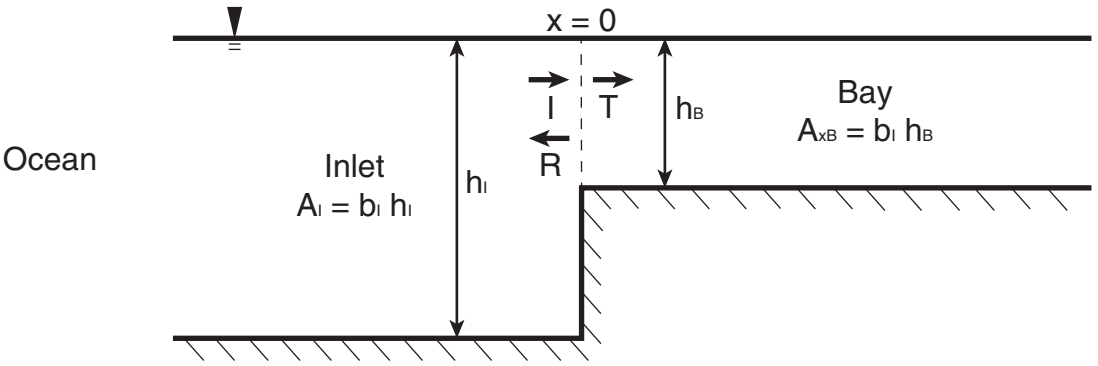

Figure A1. Schematic of a shallow bay connected to the ocean through a deeper inlet. The arrows labeled *I*, *T*, and *R* correspond to the incident, transmitted, and reflected waves, respectively. A_I is the cross-sectional area of the inlet with width b_I and depth h_I, and A_{xB} is the cross-sectional area of the bay with width (at the inlet mouth) b_I and depth h_B.

$$(a_i+a_R)(a_i-a_R)\sqrt{h_I}=a_T^2\sqrt{h_B} \tag{A5}$$

$$a_i-a_R=a_T\sqrt{\frac{h_B}{h_I}} \tag{A6}$$

where b_I is the inlet width and the subscripts i and I refer to the incident wave and the inlet location, respectively. Combining equations (A3) and (A6) yields

$$T_0=\frac{a_T}{a_i}=\frac{2\sqrt{h_I}}{\sqrt{h_B}+\sqrt{h_I}} \tag{A7}$$

$$R_0=\frac{a_R}{a_i}=\frac{\sqrt{h_I}-\sqrt{h_B}}{\sqrt{h_I}+\sqrt{h_B}} \tag{A8}$$

where the subscript 0 refers to $x=0$. Equations (A7) and (A8) describe the transmission and reflection coefficients, respectively, as functions of the depths of the inlet and bay [*Kurkin et al.*, 2015]. Using $\sqrt{gh}=c=P/z_H$, equations (A1), (A3) and (A4) lead to

$$z_{HI}\frac{\rho g(a_i+a_R)}{\rho g(a_i-a_R)}=z_{HB}\frac{\rho g a_T}{\rho g a_T}=z_{HB} \tag{A9}$$

where z_{HI} and z_{HB} are the specific hydrodynamic impedances of the inlet and bay, respectively. To remove the dependence of the amplitude coefficients, a_*, the reflection coefficient, R_0, can be defined in terms of impedance, and equation (A9) becomes

$$z_{HI}(a_i+a_R)=z_{HB}(a_i-a_R)$$

$$a_i(z_{HI}+z_{HB})=a_T(z_{HB}-z_{HI})$$

$$z_{HI}=z_{HB}\frac{1-R_0}{1+R_0} \tag{A10}$$

Using the definition of R_0 (equation (A8)) and the definition of hydrodynamic impedance for the bay (equation (A1), where only a single wave propagates), (A10) becomes

$$z_{HI}=\rho c_B\frac{1-\frac{\sqrt{h_I}-\sqrt{h_B}}{\sqrt{h_I}+\sqrt{h_B}}}{1+\frac{\sqrt{h_I}-\sqrt{h_B}}{\sqrt{h_I}+\sqrt{h_B}}}=\rho c_B\sqrt{\frac{h_B}{h_I}} \tag{A11}$$

Although the formulation for hydrodynamic impedance is calculated for a progressive shallow water wave, when included in the lumped element model, the long wavelength limit $(kh \to 0)$ is used. Thus, whereas the incoming tide is progressive on a global scale, the lumped element model assumption of no spatial

changes across the bay is consistent with the small dimensions (relative to the tide) of the Katama system. The long wavelength limit does not change the reflection and transmission coefficients.

In the formulation of equation (2), the boundary condition between the inlet and bay was that the depths were equal. In this case, the boundary does not alter the flow from the inlet to the bay. In the case where the bay depth is different than the inlet depth, the hydrodynamic impedance is different, generating the reflection. To satisfy using equation (2), the boundary condition must also be satisfied (conservation of energy flux). To create an element for the lumped element model for a multiple-inlet system that satisfies the boundary conditions across the step, the impedance difference must be determined. Given the relationship $Z_*=z_*/A_*$, the impedance owing to the shallowness of the bay is defined as

$$Z_S=Z_{H,B}-Z_{H,I}=\frac{\rho c_B}{h_B b_I}-\frac{\rho c_B}{h_I b_I}\sqrt{\frac{h_B}{h_I}}=\frac{\rho c_B}{b_I h_B}\left(\frac{h_I^{3/2}-h_B^{3/2}}{h_I^{3/2}}\right) \tag{A12}$$

where $Z_{H,I}=z_{HI}/A_I$ is the hydrodynamic impedance in the inlet and $Z_{H,B}=z_{HB}/A_{xB}$ is the hydrodynamic impedance of the bay, where $A_{xB}=h_B b_I$. The step impedance, Z_S, is the excess hydrodynamic impedance at the inlet-bay boundary, and therefore satisfies the equation

$$Z_S={}^{\rho g\Delta\eta}\big/_{U_I} \tag{A13}$$

Thus, there is an additional change in sea level generated by the step (away from the boundary) to maintain conservation of mass (discharge, U_I) across the step. Water level differences between the bay and ocean at a tidal inlet also may be caused by inertia through the inlet, friction, and entrance or exit losses (neglected here) [*O'Brien and Clark*, 1975; *Mehta and Joshi*, 1988]. For $h_I=h_B$, there is no step to impede the flow and $Z_S=0$. As $h_B \rightarrow 0$ (in one inlet only), $Z_S \rightarrow \infty$, and the flow through the inlet is impeded completely, and the bay mimics the second inlet. As $h_B \rightarrow \infty$, the solution no longer is valid.

Acknowledgments
The data used in this study are available by sending an e-mail to the authors (elgar@whoi.edu, britt@whoi.edu). We thank the PVLAB field crew for tolerating too many ferry rides and for obtaining the Katama data despite sometimes arduous conditions (and some nice ones, too!). Funding was provided by ASD(R&E), NOAA Sea Grant, NSF, and ONR.

References

Brown, E. I. (1928), Inlets on sandy coasts, *Proc. Am. Soc. Civ. Eng.*, *54*(2), 505–554.
Dalrymple, R. A., and P. A. Martin (1992), Perfect boundary conditions for parabolic water-wave models, *Proc. R. Soc. London, Ser. A*, *437*, 41–54.
Dean, R. G., and R. A. Dalrymple (1991), *Water Wave Mechanics for Engineers and Scientists*, vol. 2, World Sci., N. J.
de Boer, J. P., and L. R. Maas (2011), Amplified exchange rate by tidal forcing of a piecewise-linear Helmholtz bay, *Ocean Dyn.*, *61*(12), 2061–2072.
De Swart, H. E., and N. D. Volp (2012), Effects of hypsometry on the morphodynamic stability of single and multiple tidal inlet systems, *J. Sea Res.*, *74*, 35–44.
Gill, A. (1982), *Atmosphere-Ocean Dynamics*, *Int. Geophys. Ser. 30*, 662 pp., Academic, San Diego, Calif.
Herman, A. (2007), Numerical modelling of water transport processes in partially-connected tidal basins, *Coastal Eng.*, *54*, 297–320.
Keulegan, G. H. (1951), *Third Progress Report on Tidal Flow in Entrances: Water-Level Fluctuations of Basins in Communication With Seas*, U.S. Dep. of Commer., Natl. Bur. of Stand.
Keulegan, G. H. (1967), Tidal flow in entrances; water-level fluctuations of basins in communication with seas, *Tech. Bull. 14*, Comm. On Tidal Hydraul. (Army), Washington, D. C.
Kinsler, L. E., A. R. Frey, A. B. Coppens, and J. V. Sanders (1976), *Fundamentals of Acoustics*, John Wiley, Hoboken, N. J.
Kurkin, A. A., S. V. Semin, and Y. A. Stepanyants (2015), Transformation of surface waves over a bottom step, *Izv. Atmos. Oceanic Phys.*, *51*(2), 214–223.
Lee, J. J., and X. Xing (2010), Computer modeling for harbor planning and design, in *Handbook of Coastal and Ocean Engineering*, edited by Y. C. Kim, pp. 695–722, World Scientific, N. J.
Maas, L. R. (1997), On the nonlinear Helmholtz response of almost-enclosed tidal basins with sloping bottoms, *J. Fluid Mech.*, *349*, 361–380.
Maas, L. R., and A. Doelman (2002), Chaotic tides, *J. Phys. Oceanogr.*, *32*, 870–890.
Malhadas, M. S., P. C. Leitao, A. Silva, and R. Neves (2009), Effect of coastal waves on sea level in Obidos Lagoon, Portugal, *Cont. Shelf Res.*, *29*, 1240–1250.
Mehta, A. J., and P. B. Joshi (1988), Tidal inlet hydraulics, *J. Hydraul. Eng.*, *114*(11), 1321–1338.
Miles, J. W. (1971), Resonant response of harbours: An equivalent-circuit analysis, *J. Fluid Mech.*, *46*(02), 241–265.
Miles, J. W. (1974), Harbor seiching, *Annu. Rev. Fluid Mech.*, *6*(1), 17–33.
Miles, J. W., and Y. K. Lee (1975), Helmholtz resonance of harbours, *J. Fluid Mech.*, *67*(03), 445–464.
Miles, J. W., and W. H. Munk (1961), Harbor paradox, J. Waterw. Harbors Coastal Eng. Div., Am. Soc. Civ. Eng., *87*, 111–130.
O'Brien, M. P., and R. R. Clark (1974), Hydraulic constants of tidal entrances, *Coastal Eng. Proc.*, *1*(14), 1549–1565.
Orescanin, M., B. Raubenheimer, and S. Elgar (2014), Observations of wave effects on inlet circulation, *Cont. Shelf Res.*, *82*, 37–42.
Orescanin, M. M., S. Elgar, and B. Raubenheimer (2016), Changes in Bay Circulation in an Evolving Multiple Inlet System, *Cont. Shelf Res.*, *125*, 13–22.
Pawlowicz, R., B. Beardsley, and S. Lentz (2002), Classical tidal harmonic analysis including error estimates in MATLAB using T_TIDE, *Comput. Geosci.*, *28*(8), 929–937.
Pierce, A. (1989), Acoustics: An introduction to its physical principles and applications, *J. Acoust. Soc. Am.*
Ridderinkhof, H. (1988), Tidal and residual flows in the Western Dutch Wadden Sea II: An analytical model to study the constant flow between connected tidal basins, *Neth. J. Sea Res.*, *22*(3), 185–198.

Speer, P. E., and D. G. Aubrey (1985), A study of non-linear tidal propagation in shallow inlet/estuarine systems Part II: Theory, *Estuarine Coastal Shelf Sci.*, *21*(2), 207–224.

Stanev, E. V., G. Flöser, and J. O. Wolff (2003), First-and higher-order dynamical controls on water exchanges between tidal basins and the open ocean: A case study for the East Frisian Wadden Sea, *Ocean Dyn.*, *53*(3), 146–165.

Terra, G. T., W. J. van de Berg, and L. R. M. Maas (2005), Experimental verification of Lorentz' linearization procedure for quadratic friction, *Fluid Dyn. Res.*, *36*, 175–188.

Van de Kreeke, J. (1967), Water-level fluctuations and flow in tidal inlets, *J. Waterw. Harbors Coastal Eng. Div. Am. Soc. Civ. Eng.*, *93*(4), 97–106.

Van de Kreeke, J. (1988), Hydrodynamics of tidal inlets, in *Hydrodynamics and Sediment Dynamics of Tidal Inlets*, edited by D. G. Aubrey and L. Weishar, pp. 1–23, Springer, New York.

Van de Kreeke, J., R. L. Brouwer, T. J. Zitman, and H. M. Schuttelaars (2008), The effect of a topographic high on the morphological stability of a two-inlet bay system, *Coastal Eng.*, *55*(4), 319–332.

Waterhouse, A. F., A. Valle-Levinson, and C. D. Winant (2011), Tides in a system of connected estuaries, *J. Phys. Oceanogr.*, *41*(5), 946–959.